

Time-of-flight estimation by utilizing Kalman filter tracking information – Part I: the concept

Winfried A. Mitaroff *

Institute of High Energy Physics,
Austrian Academy of Sciences, Vienna

14 September 2021

Abstract

Recent detector concepts at future linear or circular e^-e^+ colliders (HZ^0 and $t\bar{t}$ factories) emphasize the benefits of time-of-flight measurements for particle identification of long-lived charged hadrons (π^\pm , K^\pm and p/\bar{p}).

That method relies on a precise estimation of the time-of-flight as expected, for a given mass hypothesis, from the reconstructed particle momentum and its trajectory. We show that for a realistic detector set-up, relativistic formulae are a good approximation down to lowest possible momenta.

The optimally fitted track parameters are commonly defined near the interaction region. Extrapolation to a time-of-flight counter located behind the central tracking device can usually only be performed by a track model undisturbed from material effects. However, the true trajectory is distorted by multiple Coulomb scattering and the momentum is changed by energy loss. As a consequence, the estimated time-of-flight is biased by a large systematic error.

This study presents a novel approach of time-of-flight estimation by splitting the trajectory into a chain of undisturbed track elements, following as close as possible the true trajectory. Each track element possesses an individual momentum p_i and flight distance l_i . Remarkably, our formulae emerge by formally replacing the global momentum squared p^2 by the weighted harmonic mean of the individual $\{p_i^2\}$, with the weights being the corresponding individual $\{l_i\}$.

The optimally fitted parameters of the individual track elements can be obtained from track reconstruction by a Kalman filter plus smoother. However, care must be taken when including mass-dependent material effects.

Explicit formulae for a simple scenario (homogeneous magnetic field and cylindrical surfaces) are given, together with an overview about the treatment of multiple Coulomb scattering and energy loss by a Kalman filter.

A Monte Carlo study corroborating our concept will follow.

* winfried.mitaroff@oeaw.ac.at

1 Introduction

Experiments at high-energy particle colliders consist of large complex detectors surrounding the beam interaction region, for recording the signals of particles produced in the collision events. A central tracking device (CTD), operating in a magnetic field, permits geometric reconstruction of the trajectories of long-lived charged particles [1,2]. The task of particle identification (PID) consists in determining the particle type, i.e. its mass [3]. This may be achieved by several methods:

Electrons e^- and positrons e^+ are identified by electromagnetic calorimeters behind the CTD, and muons μ^\pm by dedicated counters outside the bulk of material of the detector. Identification of the hadrons π^\pm , K^\pm and p/\bar{p} are based on effects like specific energy loss dE/dx in matter, Cherenkov or transition radiation (dependent on the velocity), or by measuring the time-of-flight (TOF) [3,4].

This study investigates only algorithmic aspects of the TOF method. Hardware issues like defining “time zero”, achieving fast TOF counter signal responses, or synchronizing time stamps are beyond the scope of this paper.

Section 2 presents a general overview of the TOF method, together with examples of calculating time differences in an ideal scenario, and a discussion of problems arising from the conventional approach in realistic scenarios.

Section 3 introduces a novel approach by splitting the global trajectory into a set of smaller track elements with individual momenta, pinpointing to consequences arising from mass-dependence of material effects. This approach can be implemented by using information available from track fitting in the CTD by a Kalman filter & smoother (KFS); formulae are given for a simple detector set-up.

Section 4 gives an overview of the KFS treating with material effects.

A summary is given in section 5. Appendix 6.1 defines the units used and some relativistic variables, and 6.2 presents conventional helix tracking coordinates.

2 The time-of-flight method

The time T needed for a particle of mass m moving with velocity v or momentum p along a distance L in the “laboratory frame” is given by ¹

$$T(m) = \frac{L}{v} = \frac{L}{\beta c} = \frac{L}{c} \cdot \sqrt{1 + \eta^{-2}} = \frac{L}{c} \cdot \sqrt{1 + \frac{m^2}{p^2}} \quad (1)$$

For a relativistic particle this can be approximated as

$$p \gg m \implies T(m) \approx \frac{L}{c} \cdot \left(1 + \frac{m^2}{2p^2}\right) \quad (2)$$

First, eqs. (1) and (2) may be used to discriminate between two hypotheses about a particle’s mass being either m_1 or m_2 . Let $\Delta m^2 \equiv m_2^2 - m_1^2$. The corresponding time-of-flight difference, as a function of both L and p , is

$$\Delta T = \frac{L}{c} \cdot \left(\sqrt{1 + \frac{m_2^2}{p^2}} - \sqrt{1 + \frac{m_1^2}{p^2}} \right) \approx \frac{L}{2cp^2} \cdot \Delta m^2 \quad (3)$$

¹See appendix 6.1 for definitions of the variables and the units used.

Second, precise measurement of the time-of-flight T by a dedicated TOF counter, together with accurate estimates of the flight distance L and of the momentum p , yields an estimate for the particle's mass squared, viz.

$$m^2 = p^2 \cdot \left[\left(\frac{cT}{L} \right)^2 - 1 \right] \approx 2p^2 \cdot \left(\frac{cT}{L} - 1 \right) \quad (4)$$

$$\sigma(m^2) = 2p^2 \cdot \left(\frac{cT}{L} \right)^2 \cdot \left[\frac{\sigma(T)}{T} \oplus \frac{\sigma(L)}{L} \right] \approx 2p^2 \cdot \frac{cT}{L} \cdot \left[\frac{\sigma(T)}{T} \oplus \frac{\sigma(L)}{L} \right] \quad (5)$$

while the contribution of the error $\sigma(p)/p$ is suppressed by a factor $(cT/L - 1) \ll 1$ and therefore has been neglected in eq. (5).²

Meaningful measurements of Δm^2 require

$$\frac{\sigma(m^2)}{\Delta m^2} \approx \frac{\sigma(T)}{\Delta T} \oplus \frac{T}{L} \cdot \frac{\sigma(L)}{\Delta T} < 1 \quad \implies \quad \Delta T > \sigma(T) \oplus \frac{T}{L} \cdot \sigma(L) > \sigma(T) \quad (6)$$

which, for a flight distance L , yields an upper limit

$$p^2 \approx \frac{L}{2c} \cdot \frac{\Delta m^2}{\Delta T} < \frac{L}{2c} \cdot \frac{\Delta m^2}{\sigma(T) \oplus \frac{T}{L} \cdot \sigma(L)} < \frac{L}{2c} \cdot \frac{\Delta m^2}{\sigma(T)} \quad (7)$$

As an example, for a time resolution $\sigma(T) = 10$ ps over a flight distance $L = 2$ m, separation of $\pi \leftrightarrow K$ or $K \leftrightarrow p$ could be achieved up to momenta $p < 8.65$ GeV/ c or 14.57 GeV/ c , respectively, if neglecting the error $\sigma(L)$ on the estimated flight distance. In reality, these upper limits will be lower.

Regarding eqs. (3)–(5), the flight distance L does not only depend on the geometry of the detector set-up, but on the shape of the reconstructed trajectory as well; hence, it is also a function of the fitted track parameters, and in particular of the momentum p . This dependence $L(p, \dots)$ is calculated for a simple cylindrical detector set-up and a pure helix track model in subsection 2.1 below.

2.1 Discussion of a simple scenario

In a detector set-up as outlined in appendix 6.2, the *undisturbed trajectory* of a particle of unit charge and momentum p moving in a homogeneous magnetic field of flux density B is a helix of radius r_H and slope $\cot \vartheta$:

$$r_H = \frac{p \cdot \sin \vartheta}{K_u \cdot B}, \quad \text{with} \quad K_u = 0.29979 \frac{\text{GeV}/c}{\text{T} \cdot \text{m}} \quad (8)$$

Assuming the particle originates at the centre point and is detected by a cylindrical TOF counter situated at radius R , its flight distance is

$$L = \frac{L_T}{\sin \vartheta}, \quad \text{with} \quad L_T = 2r_H \cdot \arcsin \frac{R}{2r_H} \quad (9)$$

being the distance projected onto the transversal plane.

²The dependence $L = L(p)$ implies an indirect contribution of $\sigma(p)/p$, which is determined by the track model and the detector set-up. For example, see eqs. (8)–(9).

Momentum p and polar direction angle ϑ are known from track reconstruction in the CTD which is situated in front of the TOF counter. If in addition coordinate z_H of the hit in the TOF counter is measured with sufficient accuracy,

$$\cot \vartheta = \frac{z_H}{L_T} \quad \Longrightarrow \quad L = \sqrt{L_T^2 + z_H^2} \quad (10)$$

In order for the particle not curling back before reaching the TOF counter, its helix radius and its momentum must exceed a threshold

$$r_H > \frac{R}{2} \quad \Longrightarrow \quad p > p_{min} = R \cdot \frac{K_u \cdot B}{2 \sin \vartheta}, \quad (11)$$

hence, the projected flight distance is within $R < L_T < R \cdot \pi/2$.

The relative error of the transverse momentum $p_T = p \cdot \sin \vartheta$, estimated by a track fit, may be parametrized in the “barrel region” $|\cot \vartheta| \lesssim 1$ as quadratic addition of two terms, arising from detector resolution and multiple Coulomb scattering in CTD’s material, respectively. The relative error of the momentum p , taking into account the correlation between p_T and ϑ , may approximately be parametrized as well. Formulae are given in [1, 2] and are thoroughly discussed in [5].

However, those error formulae qualify only globally and are of little use for the track element approach of section 3 below. A realistic error treatment requires an adequate Monte Carlo study which is deferred until part II.

2.2 Example of calculating $\Delta T(p)$

Applied to the simple scenario of subsection 2.1, a numerical calculation of the time-of-flight difference $\Delta T(p)$ for $\pi^\pm \leftrightarrow K^\pm$ and $K^\pm \leftrightarrow p/\bar{p}$, respectively, is performed by using both the exact and the approximate formula in eq. (3), and assuming

- a pure helix trajectory undisturbed from any material effects,
- ideal tracking resolution (zero errors on the track parameters),
- detector geometry and magnetic field of a realistic set-up [6]:
 - $R = 1.80$ m (inner radius of a scintillation TOF counter),
 - homogeneous solenoid magnetic field of $B = 3.5$ T.

Results are plotted in below for momenta from p_{min} (see eq. (11)) up to $p = 10$ GeV/ c , and for tracks at polar angles $\vartheta = 90^\circ$ (fig. 1) and $\vartheta = 45^\circ$ (fig. 2).

In logarithmic scale and with the restriction $R < L \cdot \sin \vartheta < R \cdot \pi/2$, the dependence of $\log L(p)$ on p is very weak, and the curves follow approximately

$$\log_{10} \Delta T(p) \approx \text{const} + \log_{10} \Delta m^2 - 2 \cdot \log_{10} p \quad (12)$$

The curves of the relativistic approximation can hardly be distinguished from those of the exact formula in eq. (3), even at the lowest possible momenta. This important feature will be essential for our novel approach in section 3 below.

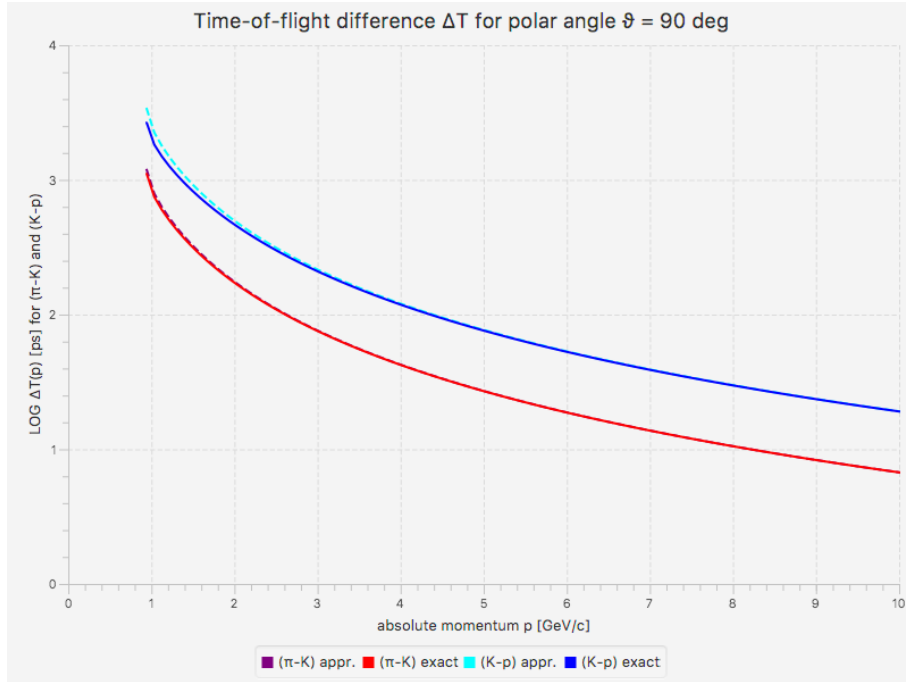


Figure 1: $\Delta T(p)$ [ps] for polar angle $\vartheta = 90^0$; logarithmic ordinate.

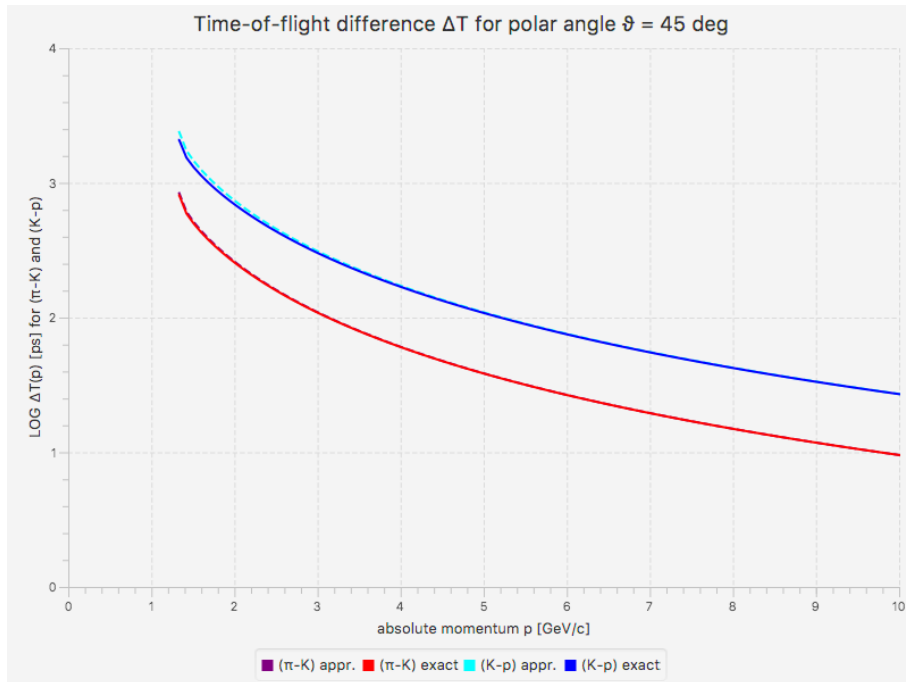


Figure 2: $\Delta T(p)$ [ps] for polar angle $\vartheta = 45^0$; logarithmic ordinate.

Figures 1 and 2: TOF differences for $\pi \leftrightarrow K$ (purple & red) and $K \leftrightarrow p$ (cyan & blue), by the exact (red/blue solid) and approximate (purple/cyan dashed) formula.

2.3 Problems in realistic scenarios

The reconstruction of a charged particle track aims at an optimal estimate of the track's 5 parameters and 5×5 covariance matrix at a pre-defined "reference location". This is achieved by an appropriate track model (imposed by the magnetic field) being fitted against the spatial measurements in the CTD, while taking into account any disturbance caused by material effects along the trajectory [1, 2].

Since the fitted track parameters are input to a subsequent vertex fit, typical reference locations are e.g. the "perigee point" w.r.t. the centre of the beam interaction profile (see appendix 6.2) or the inner surface of the beam tube (in which case propagation to the perigee point is simple). Let's call this a "type 1" fit.

Alternatively, a reference location may be chosen outside of the CTD, e.g. at the inner surface of the TOF counter, to be called "type 2" fit.

Estimation of the time-of-flight requires either outward extrapolation of the fitted track from the perigee point to the TOF counter (type 1), or inward extrapolation in the opposite direction (type 2). In the conventional approach, both are realized by simply applying the track model to an undisturbed trajectory while ignoring all matter effects in between. Then, e.g. for a homogeneous magnetic field and a cylindrical TOF counter, the flight distance can be calculated by eqs. (8)–(10).

In reality, multiple Coulomb scattering causes stochastic kinks of the 2 direction angles, and energy loss decreases the momentum p . Both effects modify the shape of the trajectory. As a result, the estimated TOF is expected to be biased by a systematic error growing larger with the detector's material budget increased.

A recent simulation study, comparing type 1 and type 2 fits of π^\pm and K^\pm tracks in a realistic detector [6], found this bias changing sign but being less significant at type 2; the behaviour of p/\bar{p} tracks was not conclusive [7].

This suggests defining a "type 3" fit as the *weighted mean*³ of type 1 and type 2, then to use its undisturbed trajectory for the conventional approach of TOF estimation [8]. We are, however, pursuing a more radical ansatz.

3 A novel approach to TOF

A possible way to solve the problems discussed in subsection 2.3 above is based on the characteristics of modern detector set-ups. The material budget in the "central region", i.e. inside of the TOF counter, is concentrated in layers which are geometrically thin w.r.t. the distances between them. From inside out, they usually consist of the beam tube; silicon pixel and/or strip layers in the vertexing part of the CTD; followed either by many layers of an all-*Si* tracker, or by a gaseous tracker (material mostly at inner and outer wall) optionally augmented by additional *Si* layers [1, 2].

This can be described by n surfaces of zero geometric thickness, though with finite material thickness expressed in radiation lengths X_0 or in g/cm^2 . All disturbances of the global track model by material effects (multiple Coulomb scattering and energy loss) can be accounted for by splitting the real trajectory into a set of $n + 1$ undisturbed track elements in front of, between, and behind those surfaces.

³Note that a weighted mean must be performed at the same reference location and must use the same set of parameters. This requires e.g. type 1 first to be propagated by the undisturbed track model to the reference location of type 2 (inner surface of the TOF counter).

Let the track elements be numbered $i = 0 \dots n$. Their individual momenta p_i and flight distances l_i are assumed to be known from reconstruction in the CTD. As has been shown in subsection 2.2 above, the corresponding travelling times t_i can be estimated according to eq. (1) or its relativistic approximation eq. (2), yielding

$$t_i(m) = \frac{l_i}{c} \cdot \sqrt{1 + \frac{m^2}{p_i^2}} \approx \frac{1}{c} \cdot \left(l_i + \frac{m^2}{2} \cdot \frac{l_i}{p_i^2} \right) \quad (13)$$

Total flight distance L and total travelling time T are

$$L = \sum_{i=0}^n l_i \quad (14)$$

$$T(m) = \sum_{i=0}^n t_i(m) \approx \frac{1}{c} \cdot \left(L + \frac{m^2}{2} \sum_{i=0}^n \frac{l_i}{p_i^2} \right) \quad (15)$$

The estimated time-of-flight difference ΔT between two hypotheses, distinguished by the difference of the masses squared Δm^2 , is given by

$$\Delta T \approx \frac{\Delta m^2}{2c} \sum_{i=0}^n \frac{l_i}{p_i^2} \quad (16)$$

And an estimate of the particle mass squared yields

$$m^2 \approx 2 \langle p^2 \rangle_{HM} \cdot \left(\frac{cT}{L} - 1 \right), \quad \text{with } \langle p^2 \rangle_{HM} \equiv \sum_{i=0}^n l_i / \sum_{i=0}^n \frac{l_i}{p_i^2} \quad (17)$$

being the *weighted harmonic mean* of $\{p_i^2\}$, in which the weights are given by the corresponding flight distances $\{l_i\}$. Similar as for eq. (5), the contribution of the error $\sigma(\langle p^2 \rangle_{HM})$ is suppressed by a factor $(cT/L - 1) \ll 1$, hence the error on m^2 is dominated by the measurement errors $\sigma(T)$ and $\sigma(L)$ alone, viz.

$$\sigma(m^2) \approx 2 \langle p^2 \rangle_{HM} \cdot \frac{cT}{L} \cdot \left[\frac{\sigma(T)}{T} \oplus \frac{\sigma(L)}{L} \right] \quad (18)$$

By comparison, it is remarkable that eqs. (15)–(18) can be derived from eqs. (2)–(5) just by formally replacing

$$\frac{L}{p^2} \rightarrow \sum_{i=0}^n \frac{l_i}{p_i^2} \quad \Longrightarrow \quad p^2 \rightarrow \langle p^2 \rangle_{HM} \quad (19)$$

Remarks about the novel approach

A necessary pre-requisite for this approach to work is knowledge of the optimally fitted track parameters at all n surfaces as reference locations. This can be achieved by a Kalman filter with smoother (KFS),⁴ see subsection 3.1 below.

⁴The resulting individual p_i will be strongly correlated.

If energy loss may be neglected, the momentum stays unchanged, i.e. $p_i = p$ for all i . In this case, only eq. (14) remains relevant, accounting for the zig-zag trajectory caused by multiple scattering; eqs. (15)–(18) revert to (2)–(5).

Multiple scattering at low momenta ($\beta < 1$) and energy loss are dependent on the particle’s mass m , see section 4. Consequently, if those effects are to be included, the KFS must be performed *separately for each mass hypothesis*. This affects above approach, eqs. (14)–(18): the $\{l_i\}$ and $\{p_i\}$ result from different KFS fits, implying that $L = \sum l_i$ and $\sum(l_i/p_i^2)$ become implicitly dependent on m , viz.

$$L(m) = \left[\sum_{i=0}^n l_i \right]_m \quad (20)$$

$$T(m) \approx \frac{1}{c} \cdot \left(L(m) + \frac{m^2}{2} \left[\sum_{i=0}^n \frac{l_i}{p_i^2} \right]_m \right) \quad (21)$$

$$\Delta T = T(m_2) - T(m_1) \quad (22)$$

replacing eqs. (14)–(16). Alas, no simple explicit expression for an estimate of the particle mass squared (like in eqs. (17)–(18)) can be given anymore.

3.1 Kalman filter and smoother

The track model is in general highly non-linear, e.g. a helix to intersect plane or cylindrical surfaces. Therefore fitting is not exerted on the track parameters directly, but on a linear expansion of their deviation from a “reference track” to be chosen as close as possible w.r.t. the true trajectory in order to maintain linearity.

State-of-the-art in track fitting is based on the Kalman filter (KF), a recursive and locally linear estimator.⁵ Multiple scattering is regarded “process noise”, but energy loss constitutes a change of the track model. The optimal estimate is achieved after the final filter step, and is equivalent to a global least squares fit.

One asset of the KF is its ability to be supplemented by a “smoother” providing optimal track fit estimates along all previous filter steps. Detailed formulae for implementing a KF with smoother (KFS) are listed e.g. in [1] and [2]. Explicit instructions for implementing material effects are given in section 4.

The “reference surfaces” defining the steps of a KFS can be classified as:

1. Active surface of zero material thickness, contributing position measurements only (e.g. “virtual cylinders” spanned by the cathode pad-rows of a TPC [1]);
2. Passive surface of finite material thickness, without measurement information (beam tube, inner and outer wall of a gaseous detector, support structure, etc);
3. Active & passive surface combined (single- or double-sided silicon layer).

Numbering the reference surfaces S_i ($i = 1 \dots n$) outward along the trajectory, which is represented by a chain of track elements φ_i between S_i and S_{i+1} , each φ_i is defined by the smoothed parameter vector and its covariance matrix located at surface S_i (in case of

⁵Robustification, e.g. by adaptive filters, is however non-linear.

class 2 or 3, take the one at the “outside face”) and follows the undisturbed track model. Adjacent elements \wp_i^* (\wp_{i-1} propagated to the “inside face” of S_i) and \wp_i are connected at surface S_i without spatial displacement, but with a kink in the direction angles and differing momenta in case of a class 2 or 3 surface.⁶

Applying the KFS to the track element approach eqs. (13)–(17), the momentum p_i can be derived from the track parameters of \wp_i , and the flight distance l_i can be calculated by extrapolation of $\wp_i \rightarrow \wp_{i+1}^*$ to surface S_{i+1} with help of the undisturbed track model. The final target surface S_{n+1} is the TOF counter.

The starting track element \wp_0 is derived from the optimal track fit at the perigee point. This is reasonable for all tracks originating from the primary or a short-lived secondary vertex. Tracks from the long-lived decays $K_S^0 \rightarrow \pi^+\pi^-$ and $\Lambda^0 \rightarrow p\pi^-$ are characterized by a large transverse impact parameter $|\delta_T|$ and can easily be identified by their “V zero” topology, hence do not require additional PID.

3.2 Applied to the simple scenario

Reverting to the simple scenario of subsection 2.1, described by a homogeneous magnetic field B and cylindrical reference surfaces S_i at radii R_i ($i = 1 \dots n + 1$), modify the track model from a single undisturbed trajectory to one based on track elements \wp_i ($i = 0 \dots n$) defined by the smoothed track fit results of a KFS.

As shown in appendix 6.2, the five track parameters (2 positions, 2 directions, and one inverse proportional to the momentum) can be defined by choice. Let’s denote our smoothed parameter vector of track element \wp_i at R_i by $\wp_i = [\Phi_i, z_i, \vartheta_i, \varphi_i, \Upsilon_i]$, with $\Upsilon_i = \kappa_i$ or $Q/(p_T)_i$ or Q/p_i . In case of a different parametrization provided by the KFS, they can be derived by an appropriate transformation. For the perigee parameters w.r.t. a pivot point at the origin, set $R_0 = |\delta_T|$, $z_0 = \delta_z$.

Calculation of the momenta p_i and flight distances l_i , as required by eqs. (14)–(18), follows from eqs. (8)–(10) and appendix 6.2 as

$$p_i = \frac{(p_T)_i}{\sin \vartheta_i} = \frac{K_u \cdot B}{|\kappa_i| \cdot \sin \vartheta_i}, \quad \text{with helix radius} = 1/|\kappa_i| \quad (23)$$

$$l_i = \frac{\varphi_{i+1}^* - \varphi_i}{|\kappa_i| \cdot \sin \vartheta_i} = \sqrt{\left(\frac{\varphi_{i+1}^* - \varphi_i}{\kappa_i}\right)^2 + \left(z_{i+1} - z_i\right)^2} \quad (24)$$

with φ_{i+1}^* being the smoothed azimuthal direction at the “inside face” of a class 2 or 3 surface S_{i+1} , otherwise $\varphi_{i+1}^* = \varphi_{i+1}$. Alternatively, using the cosine rule, the azimuthal directions may be replaced by the azimuthal positions:

$$\varphi_{i+1}^* - \varphi_i = 2 \arcsin \left(\frac{|\kappa_i|}{2} \cdot \sqrt{R_{i+1}^2 - 2R_{i+1}R_i \cos(\Phi_{i+1} - \Phi_i) + R_i^2} \right) \quad (25)$$

Eqs. (23)–(25) will be used for the Monte Carlo study of part II.

Side remark about non-helix tracking

In case of an inhomogeneous magnetic field requiring a track model based on stepwise integration by the Runge-Kutta (RK) method [2], the individual flight distances $\{l_i\}$ are automatically calculated along with the integration steps.

⁶If energy loss can be neglected, the momenta remain equal.

4 Kalman filter with material

Track fitting by a Kalman filter (KF) and smoother [1, 2] consists of the stages
 (A) a *forward KF* running either outward or inward through steps $k = 1 \dots n$;
 (B) a *backward KF* running in the opposite direction, i.e. steps $k = n - 1 \dots 1$;
 (C) the *smoother*, performing at each reference surface S_k ($k < n$) a weighted mean of
 A's filtered estimate $\tilde{\varphi}_k$ with B's predicted estimate $\tilde{\varphi}_{k,B}^{k+1}$, yielding the smoothed
 estimate $\tilde{\varphi}_k^n$ which represents the optimally fitted track parameters at S_k .

In subsection 3.1 surfaces are labelled S_i ($i = 1 \dots n$) outward, hence $i = k$ in case of the forward KF running outward, or $i = n - k + 1$ in the other case. Anticipating material layers, the smoothed estimates $\tilde{\varphi}_i^n$ are denoted φ_i^* or φ_i when located at the inside or the outside face of S_i , respectively ($\varphi_i^* = \varphi_i$ only if surface S_i is of class 1).

Material effects are subject to the Kalman filters of stage A and B. Formulae given below for the forward KF apply analogously also for the backward KF.

The filtered estimates have large errors at early steps k , and get increasingly accurate while adding more and more measurements in the course of the currently running filter stage A or B. This is a handicap concerning the accuracy of the inputs p_k for calculating the material effects, i.e. multiple scattering and energy loss (see below).

Optimal estimates at all intermediate steps $1 \dots n$ are eventually available only after the smoother has been performed. A possible improvement can be achieved by performing the Kalman filter & smoother (KFS) stages A–C in two iterations:

The 1st iteration proceeds as usual. But the forward and backward Kalman filters of the 2nd iteration now utilize the *smoothed estimates* $\tilde{\varphi}_k^n$ (momenta p_k) of the 1st iteration as input for the calculation of multiple scattering and energy loss [8].

The detector model of section 3 relies on layers of zero geometric but finite material thickness d_k , expressed in $[d] = X_0$ radiation lengths or in $[d] = \text{g/cm}^2$ areal mass density. The predicted parameters $\tilde{\varphi}_k^{k-1}$, Cartesian momentum \vec{p}_k and unit direction $\vec{u}_k = \vec{p}_k/p_k$ are defined at a position on the reference surface S_k where the unit normal vector be \vec{n}_k . With $\alpha_k = \angle(\vec{u}_k, \vec{n}_k)$ in space, the traversing length through layer S_k is

$$\Delta s_k = \frac{d_k}{\cos \alpha_k}, \quad \text{with} \quad \cos \alpha_k = \vec{u}_k \cdot \vec{n}_k \quad (26)$$

In the simple scenario of subsection 3.2 with parameters $\tilde{\varphi}_k^{k-1} = [\Phi_k, z_k, \vartheta_k, \varphi_k, \Upsilon_k]$ defined at a cylindrical surface of radius R_k (see appendix 6.2),

$$\cos \alpha_k = \begin{pmatrix} \sin \vartheta_k \cos \varphi_k \\ \sin \vartheta_k \sin \varphi_k \\ \cos \vartheta_k \end{pmatrix} \cdot \begin{pmatrix} \cos \Phi_k \\ \sin \Phi_k \\ 0 \end{pmatrix} = \sin \vartheta_k \cdot \cos(\varphi_k - \Phi_k) \quad (27)$$

and for the parametrization $\tilde{\varphi}_k^{k-1} = [u_k, v_k, (t_x)_k, (t_y)_k, \Upsilon_k]$ defined at a plane surface $\vec{n}_k = [0, 0, 1]$ (cf. “case 3” in subsections 4.1 and 4.2 below),

$$\cos \alpha_k = \cos \vartheta_k = 1 / \sqrt{(t_x)_k^2 + (t_y)_k^2 + 1} \quad (28)$$

both independent of the choice of the 5th parameter Υ_k . For facilitating calculations involving material effects, it will often be chosen as $\Upsilon_k = Q/p_k$ with charge $Q = \pm 1$. In case of a different parametrization by the KFS, care must be taken for properly transforming the parameters and their covariance matrix $\mathbb{C}_k^{k-1} = \text{cov}(\tilde{\varphi}_k^{k-1})$.

4.1 Multiple Coulomb scattering

Multiple Coulomb scattering off nuclei (MS) is a stochastic process that can be described by two projections $(\theta_{xz}, \theta_{yz})$ of the scattering angle θ in a local trihedron (z' pointing in the incident direction). Their core distributions are Gaussian,⁷ uncorrelated, with zero mean and variances given by the Rossi-Greisen formula [9]:⁸

$$\begin{aligned}\mathbb{E}(\theta_{xz}) &= \mathbb{E}(\theta_{yz}) = 0 \\ \sigma^2(\theta_{xz}) &= \sigma^2(\theta_{yz}) = \frac{\Delta s_k}{X_0} Q^2 \left(\frac{E_0}{\beta_k p_k} \right)^2, \quad \text{with } E_0 \approx 0.0136 \text{ GeV} \\ \text{cov}(\theta_{xz}, \theta_{yz}) &= 0\end{aligned}\tag{29}$$

introducing an often overlooked mass-dependence by the factor $1/\beta_k^2 = 1 + m^2/p_k^2$, which may only be neglected for relativistic particles, i.e. $\beta_k \approx 1$.

Orientation of the local trihedron (x', y', z') around z' is free and can be chosen such that x', z' and global z are in a plane. Transformation to global polar coordinates yields the additional variances on the direction angles caused by MS,

$$\sigma^2(\Delta\vartheta) = \sigma^2(\theta_{xz}), \quad \sigma^2(\Delta\varphi) \approx \frac{\sigma^2(\theta_{yz})}{\sin^2\vartheta}, \quad \text{cov}(\Delta\vartheta, \Delta\varphi) = 0\tag{30}$$

MS is unbiased “process noise” of covariance \mathbb{Q}_k in the system equation of a KF [1, 2]. Let $\tilde{\varphi}_k^{k-1}$ be the predicted parameter vector and $\mathbb{C}_k^{k-1} = \text{cov}(\tilde{\varphi}_k^{k-1})$ be its covariance at the front face of a zero-thickness passive (class 2 or material part of class 3) surface S_k . Then passing through S_k results in an update at the rear face,

$$\begin{aligned}\tilde{\varphi}_k &= \tilde{\varphi}_k^{k-1} \\ \mathbb{C}_k &= \mathbb{C}_k^{k-1} + \mathbb{Q}_k\end{aligned}\tag{31}$$

i.e. the parameter vector remains unchanged, whereas the covariance matrix is augmented by the noise term \mathbb{Q}_k according to the parametrization chosen.

Case 1: $\tilde{\varphi}_k^{k-1} = [\Phi_k, z_k, \vartheta_k, \varphi_k, \Upsilon_k]$, $\Upsilon_k = Q/p_k$

$$\mathbb{Q}_k = \text{diag} [0, 0, \sigma^2(\Delta\vartheta), \sigma^2(\Delta\varphi), 0]\tag{32}$$

i.e. only the diagonal elements of the (2×2) sub-matrix of direction angles (ϑ, φ) are “blown up”. Note that covariance $(\mathbb{Q}_k)_{3,5} = \text{cov}(\Delta\vartheta, \Upsilon_k) = 0$.

Case 2: $\tilde{\varphi}_k^{k-1} = [\Phi_k, z_k, \vartheta_k, \varphi_k, \Upsilon'_k]$, $\Upsilon'_k = Q/(p_T)_k \propto \kappa_k$

$$\mathbb{Q}_k = \begin{pmatrix} 0 & 0 & 0 & 0 & 0 \\ 0 & 0 & 0 & 0 & 0 \\ 0 & 0 & \sigma^2(\Delta\vartheta) & 0 & -\Upsilon'_k \cot \vartheta_k \sigma^2(\Delta\vartheta) \\ 0 & 0 & 0 & \sigma^2(\Delta\varphi) & 0 \\ 0 & 0 & -\Upsilon'_k \cot \vartheta_k \sigma^2(\Delta\vartheta) & 0 & (\Upsilon'_k \cot \vartheta_k)^2 \sigma^2(\Delta\vartheta) \end{pmatrix}\tag{33}$$

i.e. the matrix \mathbb{Q}_k gets extra elements which only vanish if $\vartheta_k = \pi/2$. There is maximal correlation $|\rho\{(\mathbb{Q}_k)_{3,5}\}| = |\rho\{\Delta\vartheta, \Upsilon'_k\}| = 1$ for all $\vartheta_k \neq \pi/2$.

⁷Few scatterings in extremely thin material follow a Landau distribution [2].

⁸Correction factors like that of Highland are controversial and omitted here.

Case 3: $\tilde{\varphi}_k^{k-1} = [u_k, v_k, (t_x)_k, (t_y)_k, \Upsilon_k = Q/p_k]$ (see appendix 6.2)

$$\mathbb{Q}_k = \begin{pmatrix} 0 & 0 & 0 & 0 & 0 \\ 0 & 0 & 0 & 0 & 0 \\ 0 & 0 & a_k & b_k & 0 \\ 0 & 0 & b_k & c_k & 0 \\ 0 & 0 & 0 & 0 & 0 \end{pmatrix}, \quad \text{with} \quad (34)$$

$$\begin{pmatrix} a_k & b_k \\ b_k & c_k \end{pmatrix} = (t_x^2 + t_y^2 + 1)_k \begin{pmatrix} t_x^2 + 1 & t_x t_y \\ t_x t_y & t_y^2 + 1 \end{pmatrix}_k \sigma^2(\theta_{xz})$$

Note that eqs. (31)–(34) apply symmetrically to the forward and backward KF, and there is no kink introduced by this update step. The kink between the directions at either face of surface S_k emerges only after the smoother stage.

4.2 Treatment of energy loss

Energy loss (EL) of a minimal ionizing particle⁹ passing through a thin layer of material at S_k is modelled by a discrete step ΔE_k of the particle’s energy,

$$\Delta E_k = \Delta s_k \cdot \mathbb{E} \left(-\frac{dE}{dx} \right), \quad \text{with} \quad [\Delta s_k] = \text{g/cm}^2 \quad (35)$$

and the mean dE/dx determined by the Bethe-Bloch formula [9]:

$$\mathbb{E} \left(-\frac{dE}{dx} \right) \approx K_0 \cdot \frac{Z}{A} \cdot \frac{Q^2}{\beta_k^2} \cdot \left[\log \left(\frac{2 m_e \eta_k^2}{I_e} \right) - \beta_k^2 - \frac{1}{2} \delta(\eta_k) \right], \quad (36)$$

$$\text{with} \quad K_0 \approx 0.000307 \frac{\text{GeV}}{\text{g/cm}^2} \quad \text{and} \quad m_e = \text{electron mass}$$

Material-dependent are Z and A (nuclear charge and mass number), I_e (atom ionization energy),¹⁰ and the “Fermi plateau” correction $\delta(\eta_k)$ which may be neglected for $\eta_k \lesssim 70$. The Bethe-Bloch function is approximately valid for $0.1 \lesssim \eta_k \lesssim 1000$ with an accuracy $\sigma(\Delta E_k)/\Delta E_k$ of a few percent; its broad minimum is at $\eta_k \approx 3 \dots 4$.

The energy loss ΔE_k implies a discrete step of the momentum:

$$\Delta p_k = \frac{\Delta E_k}{\beta_k} = \sqrt{1 + \frac{m^2}{p_k^2}} \cdot \Delta E_k \approx \left(1 + \frac{m^2}{2p_k^2} \right) \cdot \Delta E_k \quad (37)$$

$$\sigma^2(\Delta p_k) = \frac{\sigma^2(\Delta E_k)}{\beta_k^2} = (\Delta p_k)^2 \cdot \frac{\sigma^2(\Delta E_k)}{(\Delta E_k)^2} \quad (38)$$

which constitutes an abrupt change of the track model at surface S_k .

The KF prediction at the front face of S_k be $\tilde{\varphi}_k^{k-1} = [\Phi_k, z_k, \vartheta_k, \varphi_k, \Upsilon_k]$ with $\Upsilon_k = Q/p_k$ and charge $Q = \pm 1$ (“case 1”), and its covariance matrix $\mathbb{C}_k^{k-1} = \text{cov}(\tilde{\varphi}_k^{k-1})$.

⁹Bremsstrahlung is negligible for particles heavier than e^\pm .

¹⁰Take care for using the same units for both $[I_e]$ and $[m_e]$.

Passing through the material of S_k yields an update at the rear face, with increase $+\Delta p_k$ or decrease $-\Delta p_k$ if the KF running inward or outward, respectively,

$$\tilde{\varphi}_k = [\Phi_k, z_k, \vartheta_k, \varphi_k, \Upsilon_k^U], \quad \text{with} \quad \Upsilon_k^U = \frac{Q}{p_k \pm \Delta p_k} \quad (39)$$

$$\mathbb{C}_k \approx \mathbb{C}_k^{k-1} + \text{diag} \left[0, 0, 0, 0, \frac{\sigma^2(\Delta p_k)}{p_k^4} \right] \quad (40)$$

Eqs. (39)–(40) apply analogously to “case 3” with $\tilde{\varphi}_k^{k-1} = [u_k, v_k, (t_x)_k, (t_y)_k, \Upsilon_k = Q/p_k]$. However, “case 2” with the 5th parameter $\Upsilon'_k = Q/(p_T)_k \propto \kappa_k$ yields

$$\tilde{\varphi}_k = [\Phi_k, z_k, \vartheta_k, \varphi_k, \Upsilon_k^U], \quad \text{with} \quad \Upsilon_k^U = \frac{Q}{(p_T)_k \pm \Delta p_k \cdot \sin \vartheta} \quad (41)$$

$$\mathbb{C}_k \approx \mathbb{C}_k^{k-1} + \text{diag} \left[0, 0, 0, 0, \frac{\sigma^2(\Delta p_k)}{(p_T)_k^4} \cdot \sin^2 \vartheta \right] \quad (42)$$

All parametrizations affect only the 5th parameter and its variance. Eqs. (40) and (42) assume Δp_k to be uncorrelated to $\tilde{\varphi}_k^{k-1}$, and that $\Delta p_k \ll p_k$ or $(p_T)_k$.

5 Summary

This part I of a study presents algorithmic aspects of the time-of-flight (TOF) method for particle identification in detectors at high-energy colliders.

Formulae are given for discriminating between mass hypotheses or for the measurement of a particle’s mass, and are applied to a pure helix trajectory in the simple scenario of a homogeneous magnetic field and a cylindrical TOF counter.

Plotting the numerical calculation of the TOF difference $\Delta T(p)$ between $\pi \leftrightarrow K$ and $K \leftrightarrow p$ as a function of the momentum p shows the approximate formulae for relativistic particles being adequate even for the lowest possible momenta.

The real particle trajectory, however, is disturbed by material effects (multiple Coulomb scattering and energy loss) within the detector, and a conventional TOF estimate using an undisturbed trajectory is biased by a large systematic error.

Our novel approach to TOF estimation splits the trajectory into a chain of undisturbed track elements close to the true trajectory, each with an individual momentum p_i and flight distance l_i between discrete “surfaces”. New formulae for calculating TOF estimates are given; remarkably, the old global p^2 is just replaced by the weighted harmonic mean of the individual $\{p_i^2\}$, with the weights being the individual $\{l_i\}$. If energy loss may be neglected, all individual momenta p_i are equal; nevertheless, the TOF estimate benefits from a precise calculation of the total flight distance $L = \sum l_i$.

When including multiple scattering at low momenta and/or energy loss, which are both mass-dependent, the track elements must be determined separately for each mass hypothesis, thereby affecting above formulae of TOF estimation.

The necessary input for this track element approach can easily be obtained from track reconstruction by a Kalman filter with smoother (KFS). Formulae are given again for the simple scenario of a homogeneous magnetic field and cylindrical surfaces. And an overview is given for the treatment of material effects in the KFS.

So far, the errors on the track parameters have been ignored for TOF estimation. Part II, being a follow-up to sections 3 and 4, will present a Monte Carlo study based on fast simulation and reconstruction in a realistic detector set-up. It aims at quantifying the improvements on TOF estimation by the novel approach.

Acknowledgements

Thanks are due to *Rudolf Frühwirth* and *Meinhard Regler* (HEPHY Vienna) for helpful comments and suggestions, and for a careful reading of the manuscript.

6 Appendices: formulae

Appendix 6.1 defines the units used and recalls some variables of relativistic kinematics, and appendix 6.2 presents conventional helix tracking coordinates and track parametrizations (updated version of a corresponding section in [1]).

6.1 Relativistic kinematics

We use a hybrid system of units, as is common practice in experimental particle physics. For lengths and times, SI units are used, and the vacuum speed of light is

$$c = 2.9979 \dots \cdot 10^8 \text{ m/s} = 0.29979 \dots \text{ m/ns}$$

Units of energy, momentum and mass ¹¹ are $[E] = \text{GeV}$, $[p] = \text{GeV}/c$ and $[m] = \text{GeV}/c^2$, respectively. Thus, formulae expressed in SI units get rid of factors of c by formally replacing $pc \rightarrow p$ and $mc^2 \rightarrow m$. As an example, Einstein's equation reads

$$E = \sqrt{m^2 + p^2} = \gamma \cdot m \tag{43}$$

A motion of velocity \vec{v} in some inertial frame is described by the variables

$$\begin{aligned} \beta &\equiv \frac{v}{c} = \sqrt{1 - \gamma^{-2}} = \frac{1}{\sqrt{1 + \eta^{-2}}} = \frac{p}{E} \\ \gamma &\equiv \frac{1}{\sqrt{1 - \beta^2}} = \sqrt{1 + \eta^2} = \frac{E}{m} \quad (\text{Lorentz factor}) \\ \eta &\equiv \beta \cdot \gamma = \frac{\beta}{\sqrt{1 - \beta^2}} = \sqrt{\gamma^2 - 1} = \frac{p}{m} \quad (\text{“boost”}) \end{aligned} \tag{44}$$

where v, p, β and η denote the absolute values of the corresponding vectors.

¹¹The term “mass” is understood to be the “rest mass”; the notion “relativistic mass” is unnecessary, confusing, and should consistently be avoided. See also [10].

6.2 Helix tracking coordinates

The tracking detector layout is assumed to be approximately rotational symmetric w.r.t. the z -axis, but not necessarily mirror symmetric w.r.t. the origin $z = 0$. The axes (x, y, z) define a right-handed orthogonal basis of detector-global coordinates. Orientation of the x -axis is free and may be chosen by convention.

Surfaces are modelled in the radial (“barrel”) region as either cylinders of radius R or as prism planes parallel to the z -axis, and in the forward/backward regions as planes either normal to or inclined w.r.t. the z -axis. The boundary between those depends on the set-up; in z -symmetric detectors it is often around a polar angle $\vartheta \approx \pi/4$. The surfaces may be purely virtual, or real layers of material.

Besides Cartesian coordinates, cylindrical coordinates and spherical polar coordinates are defined for space points and/or momenta:

Space point $\vec{x} = [x, y, z]_{\text{cart}} = [u, v, z]_{\text{local}} = [R, \Phi, z]_{\text{cyl}}$

$$\begin{aligned} x &= R \cdot \cos\Phi & R &= \sqrt{x^2 + y^2} \\ y &= R \cdot \sin\Phi & \Phi &= \arctan(y/x), \text{ azimuth angle } 0 \leq \Phi < 2\pi \end{aligned}$$

$u = u(x, y)$, $v = v(x, y)$ are local position coordinates within a plane at fixed z .¹²

Momentum $\vec{p} = [p_x, p_y, p_z]_{\text{cart}} = [p_T, \varphi, p_z]_{\text{cyl}} = [p, \vartheta, \varphi]_{\text{sph}}$

$$\begin{aligned} p_x &= p \cdot \sin\vartheta \cdot \cos\varphi & p &= \sqrt{p_x^2 + p_y^2 + p_z^2} = \sqrt{p_T^2 + p_z^2} \\ p_y &= p \cdot \sin\vartheta \cdot \sin\varphi & \vartheta &= \arccos(p_z/p), \text{ polar angle } 0 \leq \vartheta \leq \pi \\ p_T &= p \cdot \sin\vartheta & \lambda &\equiv \frac{\pi}{2} - \vartheta, \text{ dip angle } \frac{\pi}{2} \geq \lambda \geq -\frac{\pi}{2} \\ p_z &= p \cdot \cos\vartheta & \varphi &= \arctan(p_y/p_x), \text{ azimuth angle } 0 \leq \varphi < 2\pi \end{aligned}$$

In the *very forward/backward direction* $|\tan\vartheta| \lesssim 0.5$, the angles (ϑ, φ) may be replaced by the momentum’s “direction tangents” (t_x, t_y) :

$$\begin{aligned} t_x &= p_x/p_z = \tan\vartheta \cdot \cos\varphi & p_x &= p \cdot t_x / \sqrt{t_x^2 + t_y^2 + 1} \\ t_y &= p_y/p_z = \tan\vartheta \cdot \sin\varphi & p_y &= p \cdot t_y / \sqrt{t_x^2 + t_y^2 + 1} \\ t_x^2 + t_y^2 &= p_T^2/p_z^2 = \tan^2\vartheta & p_z &= p / \sqrt{t_x^2 + t_y^2 + 1} \end{aligned}$$

The *magnetic field* is assumed to be homogeneous and aligned parallel or antiparallel to the z -axis. It is defined by the flux density $\vec{B} = [0, 0, B_z]_{\text{cart}}$. This implies a helix track model, with the axis parallel to z and the slope equal to $\cot\vartheta$.

Units used are: $[length] = \text{m}$, $[angle] = \text{rad}$, $[momentum] = \text{GeV}/c$, $[B \text{ field}] = \text{T}$, and $[charge] = e$ (elementary charge). For a particle with momentum p and charge Q , the radius of the helix r_H and its conveniently signed inverse κ are

$$r_H = \frac{1}{K_u} \cdot \frac{p \cdot \sin\vartheta}{|Q \cdot B_z|} > 0, \quad \kappa = -\text{sign}(Q \cdot B_z) / r_H$$

with the unit-dependent constant (here shown for above units)

$$K_u = (10^{-9} \frac{\text{c}}{\text{m/s}}) \cdot \frac{[length]}{\text{m}} \frac{\text{GeV}/c}{\text{T} \cdot [length]} = 0.29979 \dots \frac{\text{GeV}/c}{\text{T} \cdot \text{m}}$$

The sign convention corresponds to $\text{sign}(\kappa) = \text{sign}(d\varphi/ds) \equiv \text{sense of rotation in the } (x, y)\text{-projection}$. Note that in the absence of matter, p and ϑ are constants of motion; in case of multiple scattering but no energy loss, p remains constant.

¹²Local position coordinates $u(x', y')$, $v(x', y')$ may be given for a general plane defined by origin \vec{x}_0 and local basis vectors (\vec{e}_1, \vec{e}_2) , viz. $\vec{x} = \vec{x}_0 + x' \vec{e}_1 + y' \vec{e}_2$.

The *helix equations of motion* for a starting point $[x_S, y_S, z_S]$ and a starting azimuthal direction angle φ_S , as functions of the running parameter φ , are:

$$\begin{aligned} x(\varphi) &= x_S + (\sin\varphi - \sin\varphi_S) / \kappa \\ y(\varphi) &= y_S - (\cos\varphi - \cos\varphi_S) / \kappa \\ z(\varphi) &= z_S + \cot\vartheta \cdot (\varphi - \varphi_S) / \kappa, \quad \text{path length } s(\varphi) = (\varphi - \varphi_S) / (\kappa \cdot \sin\vartheta) \end{aligned}$$

A track fitter's 5 *internal track parameters* are defined by 2 positions, 2 directions, and one proportional to the curvature κ ,¹³ and are conveniently chosen according to the track characteristics and the geometry of the detector set-up, e.g.

$$\begin{aligned} [R\Phi, z, \cot\vartheta, \varphi - \Phi, \kappa] & \quad \text{at } R = R_S, \quad \backslash \\ [\Phi, z, \vartheta, \varphi, Q/p_T] & \quad \text{at } R = R_S, \quad \} \text{ in the radial ("barrel") region;} \\ [\Phi, z, \vartheta, \varphi, Q/p] & \quad \text{at } R = R_S, \quad / \\ [u, v, \vartheta, \varphi, Q/p] & \quad \text{at } z = z_S, \quad \text{in the forward/backward regions;} \\ [u, v, t_x, t_y, Q/p] & \quad \text{at } z = z_S, \quad \text{in the very fwd./backwd. regions,} \\ & \quad \text{with } t_x = dx/dz, t_y = dy/dz \text{ being useful for numerical tracking along } z.^{14} \end{aligned}$$

Examples of different *external track parameters* suitably chosen after inward extrapolation, to be used as "virtual measurements" for a subsequent vertex fit:

$$\begin{aligned} [x, y, z, p_x, p_y, p_z] & \quad \text{"6D Cartesian" (note that the corresponding} \\ & \quad \text{6} \times \text{6 covariance matrix is of rank 5 only);} \\ [\delta_T, \delta_z, \cot\vartheta, \Phi_0, \kappa] & \quad \text{"Perigee representation" (see below).} \end{aligned}$$

The *perigee point* $[x_0, y_0, z_0]$ of a helix track is defined, in the (x, y) -projection, as the point of closest approach (PCA) to a fixed "pivot point" $[x_P, y_P, z_P]$ which will most often be chosen at the centre of the beam interaction profile. The track parameters in perigee representation and usual convention are:

$$\begin{aligned} \delta_T &= \pm \sqrt{(x_0 - x_P)^2 + (y_0 - y_P)^2} && \text{projected distance between the} \\ & && \text{perigee and pivot points (transverse impact parameter),} \\ & && \text{with + or - sign indicating the pivot point sitting to} \\ & && \text{the left or to the right of the helix, respectively;} \\ \delta_z &= z_0 - z_P && \text{distance along } z \text{ between perigee and pivot points;} \\ \cot\vartheta & && \text{slope of the helix;} \\ \Phi_0 &= \arctan \frac{y_0 - y_P}{x_0 - x_P} && \text{azimuthal position of perigee point w.r.t. pivot point;} \\ \kappa & && \text{inverse helix radius, with the sign defined as before.} \end{aligned}$$

Alternatively, Φ_0 may be replaced by the azimuthal direction angle $\varphi_0 = \Phi_0 + \text{sign}(\delta_T) \cdot \frac{\pi}{2}$ of the helix at the perigee point.

Beware of subtle differences in various alternative conventions, e.g. for the units of length and momentum (affecting the value of K_u), the sign definitions for δ_T and κ , or a tacit assumption about $\text{sign}(B_z)$ with implicit consequences.

¹³In case of zero magnetic field \vec{B} , i.e. straight line tracks, the 5th parameter is dummy.

¹⁴Note that (t_x, t_y) alone cannot distinguish forward ($\vartheta < \pi/2$) vs. backward ($\vartheta > \pi/2$).

References

- [1] M. Krammer and W. Mitaroff: *Tracking Detectors*,
in “Handbook of Particle Detection and Imaging” (Editors: I. Fleck et al.),
2nd ed., 2021: Springer Nature, Cham (CH), DOI: 10.1007/978-3-319-47999-6
- [2] R. Frühwirth, E. Brondolin, A. Strandlie: *Pattern Recognition and Reconstruction*,
in “Particle Physics Reference Library” (Editors: C.W. Fabjan and H. Schopper),
Vol. 2 “Detectors for Particles and Radiation”,
2020: Springer Open, ISBN 978-3-030-35317-9, DOI: 10.1007/978-3-030-35318-6
- [3] R. Forty and O. Ullaland: *Particle Identification – Time-of-Flight, Cherenkov and
Transition Radiation Detectors*,
in “Particle Physics Reference Library” (Editors: C.W. Fabjan and H. Schopper),
Vol. 2 “Detectors for Particles and Radiation”,
2020: Springer Open, ISBN 978-3-030-35317-9, DOI: 10.1007/978-3-030-35318-6
- [4] W. Klempt: *Review of particle identification by time-of-flight techniques*,
Nucl.Instr.Meth. A 433 (1999) 542 - 553.
- [5] M. Valentan, M. Regler and R. Frühwirth: *Generalization of the Gluckstern
formulas II: Multiple scattering and non-zero dip angles*,
Nucl.Instr.Meth. A 606 (2009) 728 - 742.
- [6] The ILD Collaboration (Editors: T. Behnke et al.):
International Large Detector – Interim Design Report (March 2020),
DESY 20-034, KEK 2019-57, arXiv:2003.01116 [physics.ins-det]
- [7] B. Dudar et al., in “Proc. 22nd Int. Workshop on Future Linear Colliders”,
(Editor: J.E. Brau), Online 15 - 18 March 2021, arXiv:2105.12495 [hep-ex]
- [8] M. Regler (HEPHY Vienna): private communication.
- [9] H. Bichsel, D.E. Groom and S.R. Klein: *Passage of Particles Through Matter*,
in “2018 Review of Particle Physics” (Editors: M. Tabanashi et al.),
Phys.Rev. D 98, 030001 (2018) 446 - 460, DOI: 10.1103/PhysRevD.98.030001
- [10] Lev B. Okun: *The concept of mass*, Physics Today 42 (1989) 31 - 36.